energies

MDPI

Article

Optimization Design for Receiving Coil with Novel Structure Based on Mutual Coupling Model in Wireless Power Transmission for Capsule Endoscope

Shuai Kuang [1,2,*], Guozheng Yan [1,2] and Zhiwu Wang [1,2]

[1] Department of Precise Medical Engineering and Intelligent Electronic Microsystems, Shanghai Jiao Tong University, Shanghai 200240, China; gzhyan@sjtu.edu.cn (G.Y.); zwwang@sjtu.edu.cn (Z.W.)

[2] Institute of Medical Robotics, Shanghai Jiao Tong University, Shanghai 200240, China

* Correspondence: alex222@sjtu.edu.cn; Tel./Fax: +86-021-34204434

Received: 4 July 2020; Accepted: 26 November 2020; Published: 7 December 2020

Abstract: Wireless capsule endoscope (WCE) is a promising technology for noninvasive and painless imaging detection on gastrointestinal (GI) diseases. On the other hand, conventional endoscopes with wires could discomfort patients and cause them to vomit and aerosolize coronavirus if the patients are infected with COVID-19. However, there stands a technical bottleneck on power supply for the WCE. With the help of wireless power transmission technology, a hollow receiving coil (RC) is proposed to supply sufficient power and also minimize the size of WCE. A model on mutual inductance between transmitting and receiving coils is proposed to evaluate receiving power when the RC is in a different position and direction of patient's GI tract. Based on the model, an optimal RC is built to obtain sufficient and stable power. Measurement of mutual inductance with the optimal RC validates high accuracy of the proposed model. The standard deviation of receiving power is very low. WCE with optimum RC gets sufficient power and captures images stably in live pig's intestine tract. Additionally, the model is little affected by biological tissues. It ensures reliable performance of WCE and makes popular clinical application of WCE possible, which is also a relief to reduce epidemics like COVID-19.

Keywords: biomedical micro devices; gastrointestinal diseases; noninvasive endoscope; wireless capsule endoscope (WCE); wireless power transmission

1. Introduction

A wireless capsule endoscope (WCE) for detection and treatment on the gastrointestinal (GI) tract is painless, noninvasive, and portable compared to conventional endoscopes equipped with wires [1]. What's more, the conventional endoscope could discomfort patients and cause them to vomit and aerosolize corona virus like SARS-COV-2 if infected with COVID-19 [2]. WCE does not discomfort patients and is effective for reducing epidemics like COVID-19. It primarily consists of imaging, powering, communicating, and controlling circuits, and some other modules [3]. To ensure that it is swallowable and passes through the whole GI tract smoothly and safely, the diameter and length should be less than 15 and 17.5 mm, respectively [4]. To sustain normal work of WCE, it demands at least a power of 380 mW during the whole digestion period for more than 24 h [5]. It is not spatially beneficial to utilize a battery, since its power capacity per unit volume is not qualified [6]. If a battery is applied to provide sufficient power, the size of the WCE would be too large to swallow. Wireless power transmission (WPT) technology makes a sufficient power supply for micro WCEs possible [7].

WPT mainly concludes a transmitting coil (TC), a receiving coil (RC), and related circuits. A TC is worn rightly around human body, while the RC is encapsulated in WCE and works in the GI tract [8].

The main challenge for WPT on WCE lies in that RC is micro, and separated from TC with a large distance, as it is dozens of times of the size of RC [9]. They are weakly coupled with quite low power transmission efficiency [10]. Additionally, the structure and size of RC are strictly constrained within the capsule [11]. After being ingested by the patient, WCE passes through the whole GI tract, capturing images in high resolution of 400 × 400 and sending them out wirelessly [12]. Its detection scope covers the whole GI tract. By contrast, there exist some blind locations, hard to reach in the intestine for conventional endoscopes [13]. On the other hand, WCE could be in any possible position and direction in the GI tract during the detection, causing misalignment between RC and TC [14]. Thus, the receiving power varies correspondingly [15]. Solid cubic RC takes much of the space in the tiny WCE, and in some particular positions and directions, its receiving power is insufficient [16]. Solid cylindrical RC reaches a power transmission efficiency of 1% at most [17]. Meanwhile, novel functions such as auto-fluorescence imaging or drug release are promoted to increase the medical detection performance of WCE [18–20], and the power demand rises further. Above all, the geometry and configuration of RC should be specially designed to supply sufficient power for WCE.

It is too time-consuming to utilize the popular finite element method (FEM) to study receiving power of the WPT [21]. As long as misalignment alters, the FEM should be remodeled with quite high computational repetition and redundancy [22]. Its computational efficiency is low, and vital information about position and direction of WCE is not used properly. To make full use of intrinsic information about misalignments, there should be some shortcut to analyze receiving power.

In this paper, a hollow RC with novel structure is proposed so that other modules of WCE can be put inside it to save much space for WCE. Then, a model of mutual inductance between TC and RC is built to study the power issue for various misalignments of RC. It makes full use of information and characteristics of position and direction of WCE. Accuracy of the model is validated with measurement. Optimization on design parameters of the RC is implemented to ensure sufficient power even when RC is badly misaligned. Then it is put into pork tissues to infer the effect of biological tissues on the power supply of the RC. Finally, the power performance of optimal RC is verified with imaging with WCE in GI tract of live pig.

2. Methods

2.1. Novel Structure of Receiving Coil

Modules of WCE are concisely and compactly capsulate, as illustrated in Figure 1. The size of WCE is strictly tiny to get through the GI tract safely. The RC in the patient's GI tract receives power wirelessly from RC outside the body through WPT technology. Based on our early work, TC is designed as following: Current at 1A in frequency of 108 kHz, solenoid pair in diameter of 0.4 m and height of 0.2 m, and 40 turns of litz wire (180 stranded AWG38) [4,13]. It provides adequate and stable magnetic flux inside the TC, and ensures human tissues' safety at the same time. Otherwise, higher electromagnetic field or work frequency may threaten the safety of human tissues exposed to it. In certain structures and sizes, it is comfortable to wear for the patient.

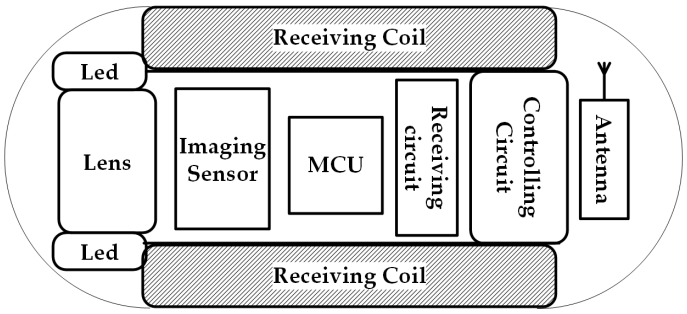

Figure 1. Overview of modules of a wireless capsule endoscope (WCE).

Meanwhile, to fit in the topology of WCE, a hollow cylinder is preferred for RC [5]. Other modules of WCE can be put inside RC to minimize the size of capsule. As illustrated in Figure 2a, the top round of the cylinder is equally divided into three groups in series. For Group 1, a litz wire comes from A_1 down to the corresponding diagonally symmetric point B_1 on the bottom round, then up back to A_2, the point right next to A_1. The single turn is in a shape of an ellipse, approximately. The second turn is wound from A_2 down to B_2, and then back up to A_3, forming another ellipse next to the first one. Other turns are implemented with the same winding. The top round of the cylinder is evenly divided into 3 N_0 points of A_1, A_2, ... , A_{3N0} by densely wound litz wire. That is, each group contains N_0 turns of coils per layer. N_0 is a decisive design parameter, which will be optimized in detail in the following section. The novel structure enables RC to receive power from three dimensions (3D). The design parameters of RC remain to be optimized to improve power performance of WCE, especially for cases of terrible misalignment between TC and RC. So, receiving power is analyzed first, and then the parameters of RC are optimized.

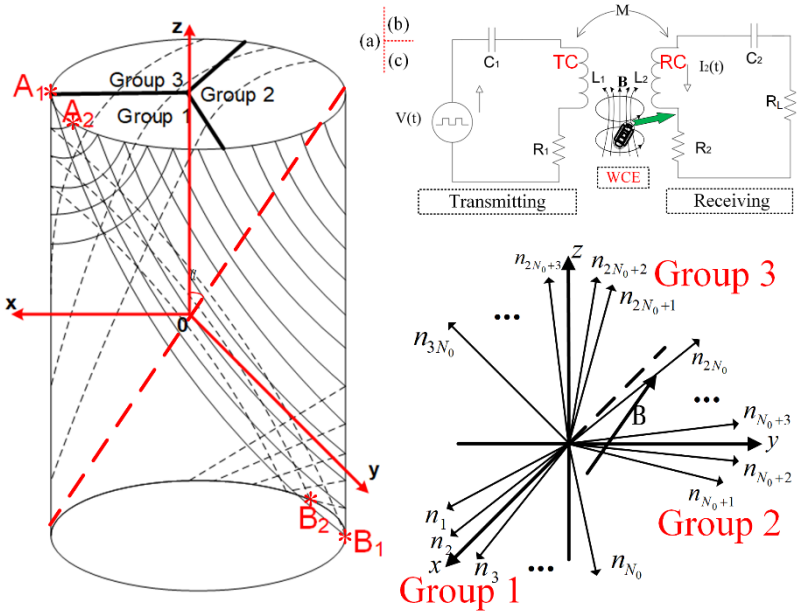

Figure 2. (**a**) Winding of hollow coil; (**b**) equivalent lumped circuit; (**c**) coordinates of normal vectors of each single turn of coil.

2.2. Model of Mutual Inductance and Receiving Power

Electrical parameters are analyzed to investigate receiving power of WCE in the lumped parameter circuit as shown in Figure 2b. R_1 and R_2, L_1 and L_2, C_1 and C_2, and Z_1 and Z_2 represent the winding resistance, self-inductance, tuning capacitor to get resonant, and equivalent impedance of TC and RC circuits correspondingly. So, impedance of TC and RC turns out to be $Z_1 = R_1 + j\omega L_1 + 1/(j\omega C_1)$ and $Z_2 = R_2 + j\omega L_2 + 1/(j\omega C_2)$, respectively. As for R_L, the load of the RC circuit in Figure 2b, turns out to be 29.72 Ω according to our previous study [18]. M is the mutual inductance between TC and RC. The angular frequency is $\omega = 2\pi f$, where f is the resonant frequency of TC and RC. Based on our previous study, for WCE, f is set as 220kHz to implement stable and sufficient WPT. There is no source voltage in the RC circuit. Its voltage is induced by TC based on an electromagnetic induction principle. Name the current in the TC circuit as $I_1(t)$, and the induced current in the RC circuit as $I_2(t)$. Magnetic hysteresis is not taken into consideration, since all related frequencies for WCE are below 10 MHz [23]. The loop equation of the WPT is:

$$\begin{pmatrix} V_1(t) \\ 0 \end{pmatrix} = \begin{pmatrix} Z_1 & -j\omega M \\ -j\omega M & R_L + Z_2 \end{pmatrix} \begin{pmatrix} I_1(t) \\ I_2(t) \end{pmatrix} \quad (1)$$

Based on Faraday's law, the induced electromotive force ε_r is:

$$\varepsilon_r = \frac{j\omega M V_1 (R_L + Z_2)}{Z_1 (R_L + Z_2) + \omega^2 M^2} \tag{2}$$

And M is:

$$M = \mu_r \mathbf{B} \cdot \mathbf{S}, \tag{3}$$

where μ_r is the relative magnetic permeability, $\mathbf{B}$ is the magnetic flux density generated by TC, $\mathbf{S}$ is the projection area of RC in the direction of the magnetic field of TC. When TC and RC are modulated to resonance to 220 kHz, there goes $\omega L_1 = 1/(\omega C_1)$ and $\omega L_2 = 1/(\omega C_2)$, and Equation (2) is transformed into:

$$\begin{pmatrix} V_1(t) \\ 0 \end{pmatrix} = \begin{pmatrix} R_1 & -j\omega M \\ -j\omega M & R_L + R_2 \end{pmatrix} \begin{pmatrix} I_1(t) \\ I_2(t) \end{pmatrix}. \tag{4}$$

The load power is [18]:

$$P_L = \frac{R_L \omega^2 M^2 V_1^2}{\left[R_1 (R_L + R_2) + \omega^2 M^2\right]^2}. \tag{5}$$

where R_1 and R_2 are calculated according to the definition of resistance. So R_1 turns out to be 1.6527Ω. Note that for different design parameters of RC, the electrical parameters L_2, C_2, and R_2 vary correspondingly. Power transmission efficiency is the ratio of the load power on RC to the motivated power from source voltage of TC, as below:

$$\eta = \frac{R_1 R_L \omega^2 M^2}{\left[R_1 (R_L + R_2) + \omega^2 M^2\right]^2}. \tag{6}$$

Based on our previous study in [4,5,13], the transmitting voltage V_1 is strictly constrained below the safety threshold to ensure electromagnetic and thermal safety issues of human tissues exposed in the electromagnetic field. According to Equations (3)–(5), in resonant state, the mutual inductance M is intrinsically decisive for receiving power. Practically, M varies all the time, since the position and direction of RC changes all the time in the patient's GI tract. The model of mutual inductance between TC and RC of WCE is proposed as follows. Considering the huge difference on magnitude between TC and RC, the magnetic flux density generated by TC can be treated as uniform inside the tiny cylinder of RC. Generally, name the magnetic flux density on the central point C of RC as $\mathbf{B}_c$. The mutual inductance between TC and each single turn of RC is studied firstly. Litz wire is selected as the winding material of RC to eliminate the electromagnetic effect of any two single turns [18]. So, for two arbitrary single turns of RC, their mutual inductance is negligible. The Cartesian coordinate system of RC is built as shown in Figure 2c. Let the unitized normal vector for each single turn of RC be $\mathbf{n}_1, \mathbf{n}_2, \ldots, \mathbf{n}_{3N_0}$, respectively. The coordinate of $\mathbf{n}_k$ turns out to be $\cos\alpha \cdot (\cos k\theta_0, \sin k\theta_0, \tan\alpha)$, where α is the angle between the diagonal and central axis of the cylinder as illustrated in Figure 2a. Additionally, α is determinative for receiving power, which will be optimized in the following section. Note the radial of the cylinder as r, and the height as h, then $\tan\alpha = 2r/h$. For each single turn k ($k = 1, 2, \ldots, 3N_0$), the major and minor axis is $2r/\sin\alpha$ and $2r$, respectively. The area of the arbitrary k-th turn is the same as $S_0 = 4\pi r^2/\sin\alpha$.

The position of the center of RC is nominated as $r_c = (x_c, y_c, z_c)$, which tells its positional displacement. The coordinates of $\mathbf{B}_c$ is $|\mathbf{B}_c| \cdot \cos\varphi \cdot (\cos\theta, \sin\theta, \tan\varphi)$, where $\theta \in [0°, 90°]$ and $\varphi \in [0°, 90°]$ stands for radially and axially directional misalignment of RC, respectively, and

$$|\mathbf{B}_C| = \frac{\mu_0 I_1}{4\pi} \left| \oint_{C_1} \frac{dl \times \mathbf{r}_C}{r_C^3} \right|. \tag{7}$$

According to the symmetry of RC, both φ and θ from 0° to 90° together cover all possible cases of directional misalignment. The mutual inductance between TC and the k-th turn of RC in the certain positional (r_c) and directional (φ and θ) misalignment is:

$$M_k = \mu_r \cdot \left|\mathbf{B_c}\right| \cdot \left|\mathbf{S}_0\right| \sigma_k(\alpha; \theta, \varphi), \tag{8}$$

where the directional factor is:

$$\sigma_k(\alpha; \theta, \varphi) = \cos\varphi \cos\alpha (\cos k\theta_0 \cos\theta + \sin k\theta_0 \sin\theta + \tan\varphi \tan\alpha). \tag{9}$$

It is determinative for the mutual inductance between TC and RC with directional misalignment. For RC with L_0 layers, the total mutual inductance between TC and the Group 1 of RC is:

$$M^1 = L_0 \sum_{k=1}^{N_0} M_k = \mu_r L_0 \cdot \left|\mathbf{B_c}\right| \cdot \left|\mathbf{S}_0\right| \cdot [\sum_{k=1}^{N_0} \sigma_k(\alpha; \theta, \varphi)] \tag{10}$$

For Group 2 and 3, M^2 and M^3 are obtained in the same way. In total, the mutual inductance between TC and RC is:

$$M = M^1 + M^2 + M^3. \tag{11}$$

Thanks to the rotational symmetry characteristic of magnetic flux density generated by TC, any axial cross section of TC equivalently covers all possible positional misalignments of RC. The cross section forms a rectangle P. To infer the actual mutual inductance of RC on all positions, let C traverse the whole P. For each position, traversal of θ and φ from 0° to 90° includes all possible directional misalignments of RC.

2.3. Optimization Design for Receiving Coil

The parameters of proposed RC are optimized to sustain normal work of WCE as follows. The primary purpose is to induce sufficient power for WCE. Receiving power P_L should be above the typical demanding power P_D. Based on our previous study, for the proposed WCE, P_D is 0.38 W, as illustrated in Table 1 [24]. Then,

$$P_L \geq 0.38. \tag{12}$$

Table 1. Power demands for each module of the capsule.

Modules	Power Demand/mW
Light source (Everlight)	30
CMOS imaging (OV6930)	65
Rectifier, regulator, and control circuits	90
Data transmission	195

Unstable or jumping power causes abnormalities such as low signal noise ratio of images or damage on components. So, the other aim is uniform and stable power performance in as many misalignment cases as possible. The standard deviation of M is introduced as M_d to depict the stability of receiving power:

$$M_d = \sqrt{\frac{1}{2hr} \int_0^h \int_0^{2r} (\frac{1}{4\pi^2} \int_0^{2\pi} \int_0^{2\pi} (M - M_{avg})^2 \, d\theta d\varphi) \, dxdz}, \tag{13}$$

where M_{avg} is the average of M for all possible positional and directional misalignments. Lower M_d indicates higher stability for receiving power. The objective function is:

$$\min \{M_d\}. \tag{14}$$

To ensure the safety of intestinal tissues near WCE, temperature rise τ of WCE caused by its heat dissipation should be under 5.5 °C [23].

$$\tau \leq 5.5. \tag{15}$$

According to Pennes' Equation, temperature rise τ is related to power as following: $P = K_T S_0 \tau$, where K_T is the heat dissipation coefficient related to the internal resistance of RC.

The WCE is swallowable when the outer diameter of RC is below 0.0125 m. Meanwhile, other circuits can be put inside the hollow RC on the condition that inner diameter is larger than 0.0065 m. So,

$$3N_0 d_0/(2\pi) \geq 0.0065, \tag{16}$$

$$d_0(\sqrt{3}(L_0 - 1)/2 + 1) + 3N_0 d_0/(2\pi) \leq 0.0125 \tag{17}$$

where d_0 is the diameter of litz wire, $d_0(\sqrt{3}(L_0 - 1)/2 + 1)$ represents the thickness of L_0 layers of wires [23].

Based on objective function of Equation (14) and constraints of Equations (5), (12) and (15)–(17), the optimization problem is built with respect to optimizing variables of N_0 (number of turns per layer for each group), L_0 (layers of RC), d_0 (wire diameter), and α (angle between diagonal and central axis of cylinder). Additionally, the optimal M_d is obtained as 1.0938 μH with genetic algorithm, where optimal design parameters of RC are $N_0 = 14$, $L_0 = 3$, $d_0 = 0.00128$ m, and $\alpha = 34.8713°$, respectively. Then, the diameter and height of RC are 0.0120 m and 0.0173 m, respectively.

3. Experimental Validation

3.1. Measurement for Mutual Inductancew with Positional or Directional Misalignment

The accuracy of the mutual inductance model when there is positional and directional misalignment on RC is verified with a measurement platform as below. The TC of the WPT system is built as referred, as shown in Figure 3. The RC with optimal design parameters is wound and put in the TC. Lumped parameters in Equation (1) are measured by HIOKI 3532-50 LCR HITESTER. L_1, L_2 are measured as 1066.0237 μH and 202.21 μH, respectively. C_1, C_2 are 0.4909 nF and 2.5882 nF, respectively. In resonant state, Z_1, Z_2 are reduced to R_1, R_2, of which the measurements are 1.7194 Ω and 27.5014 Ω, respectively. The position of the center point of RC is set to (0, 0.005i, 0.005j) orderly by the device in Figure 3, where radial $i = 0, 1, \ldots, 40$, and axial $j = 0, 1, \ldots, 30$. Additionally, RC is parallel with TC, without directional misalignment. The induced electromotive force is measured by digital multimeter Agilent 34410A. Based on Equation (2), the measurement of mutual inductance is inferred and obtained as in Figure 4b as a contrast to the calculation with the proposed model in Figure 4a. It indicates that the maximum of calculation from the proposed model (of 5.7862 μH) is a little bit less than that of the measurement (of 5.8223 μH), while the minimum of calculation (of 2.5263 μH) is more than that of the measurement (of 2.2738 μH). The proposed model slightly smooths the actual mutual inductance due to the assumption that electromagnetic interaction between any two single turns of RC is ignorable, which could be improved in future research. The root mean square error between measurement and calculation of Equation (11) in the proposed model for various positional misalignments of RC is 0.2238 μH, which indicates the high accuracy of the proposed model overall. Additionally, the error caused by the assumption is minor. When there is no directional misalignment, the standard deviation of measured mutual inductance for all positional misalignments is 1.3194 μH. It is bit higher than the calculated outcome of optimization problem (of 1.1283 μH), which is reasonable and tolerable due to

discretization error from measurement. So, the receiving power for different positional misalignments of RC is stable and basically sufficient.

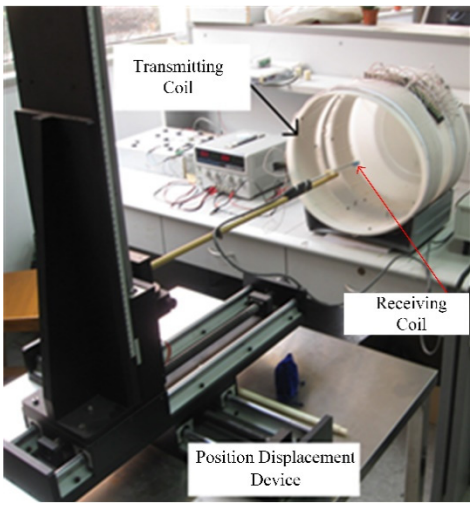

Figure 3. Setup for measuring mutual inductance when the receiving coil (RC) is in different positions.

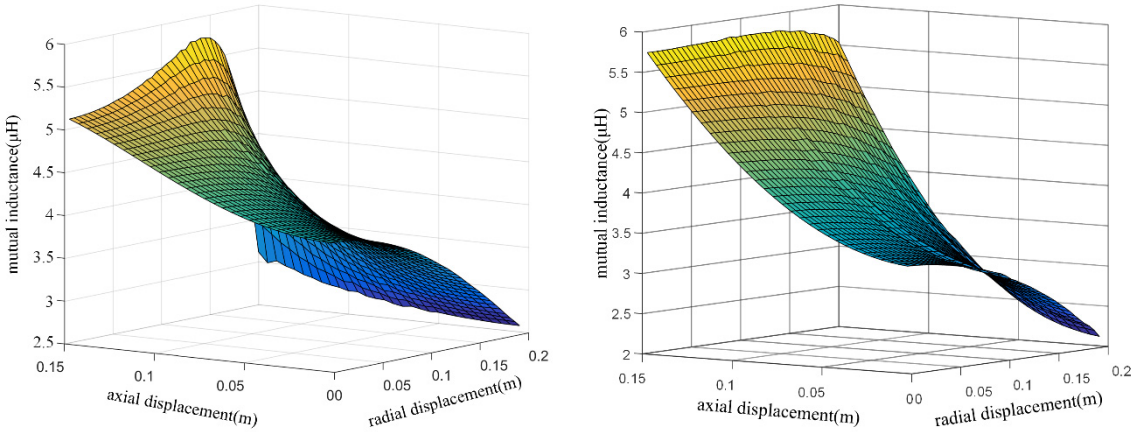

Figure 4. Mutual inductance when the receiving coil is in axial and radial displacement without directional misalignment from: (**a**) Calculation; (**b**) measurement.

At the position of (0, 0.10, 0.06 m), the RC in different directional misalignments of (θ, φ) is accomplished by a directionally rotational device as illustrated in Figure 5. The calculated and measured mutual inductance when RC is in a different direction is shown in Figure 6a,b, respectively. It indicates that the maximum of calculation with the proposed model (of 5.7862 μH) is slightly lower than that of the measurement (of 5.8221 μH), while the minimum of the model (of 1.2493 μH) is higher than that of the measurement (of 0.9628 μH). It attributes to the same assumption as referred to in the last section. The root mean square error between measurement and the proposed model is 0.2475 μH, indicating good agreement between them. The standard deviation of measured mutual inductance for all directional misalignments is 1.1747 μH. It is a little bit higher than the calculated result of the proposed model (of 1.0893 μH). It tells us that receiving power is relatively smooth and stable without an intolerably high gradient for various directional misalignments. These all benefit from the special structure and geometry of the optimal and novel RC. The 3D structure of RC ensures that at least one dimension (1D) of it is well coupled with TC, no matter how badly misaligned the RC is.

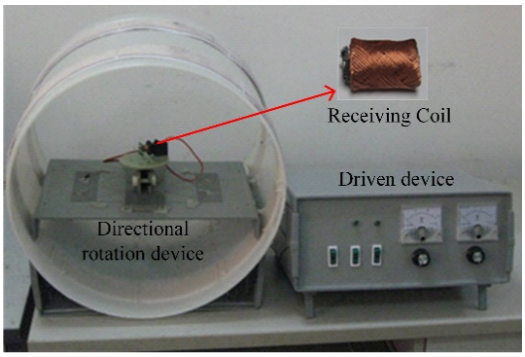

Figure 5. The Setup for measuring mutual inductance when the receiving coil is in different directions.

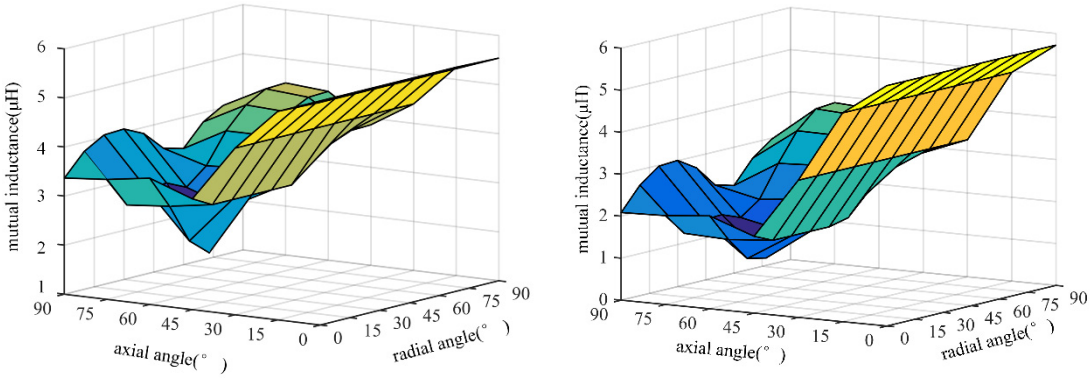

Figure 6. Mutual inductance when the receiving coil is in directional misalignment from: (**a**) Calculation with the proposed model; (**b**) measurement.

3.2. Imaging in Live Pig's Gastro-Intestine by Capsule Endoscope

WCE should be clinically applied into patients' intestine. So, the effect of biological tissues on the receiving power of the optimized RC is studied as below. WCE with the optimal RC is swallowed by a live pig, before which it gets fasted for 12 h to empty its GI tract for better imaging. It gets anesthetic and sleeps quietly inside TC, as illustrated in Figure 7. No hurt or damage happens to it during the whole experiment. All procedures complied with the Institutional Animal Use and Care Committee of Shanghai Jiao Tong University.

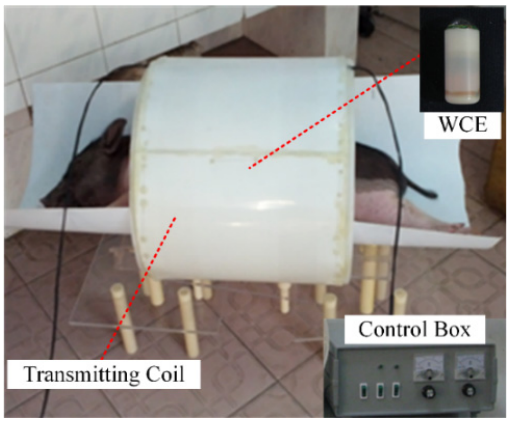

Figure 7. The setup for imaging the GI tract of live pigs with capsule endoscope.

The WCE could be in any position and direction in the pig's tract. If power is insufficient, the WCE will malfunction, and image quality will go down rapidly or even no image will display. Actually,

during the whole detection process, imaging by WCE is clear and fluent, from which two frames are stochastically sampled as illustrated in Figure 8. It indicates that WCE works normally and receiving power of the optimal RC is sufficient and stable.

Figure 8. Randomly sampled WCE images of the pig's gastrointestinal tract.

3.3. *Effect of Biological Tissues on Mutual Coupling and Wireless Power Transmission*

Detailed effects of biological tissues on mutual inductance are studied quantitatively below. As for the imaging experiment on a live pig in the previous section, the mutual inductance corresponding to certain misalignment of RC is difficult to measure in real time in the pig's GI tract. An ex vivo experiment is carried out to quantitatively study the effect of biological tissues on mutual inductance, where RC is tightly surrounded by pork tissues, as in Figure 9. There is no routine for magnetic flux between TC and RC other than penetrating through pork tissues. Mutual inductance is measured when RC is set in the positional displacement of $(0, 0.01i, 0)$ orderly, where $i = 0, 1, \ldots, 8$, without directional misalignment. It is compared with calculations of the proposed model and measurement without biological tissues in the previous section, as illustrated in Figure 10. Errors between calculation of the proposed model and measurement with biological tissues in this section are higher than those between calculation of the model and measurement without biological tissues in the previous section. It indicates that biological tissues do weaken the mutual inductance to some degree. However, errors between measurement with and without tissues (curve b and c) are tolerable, significantly smaller than errors between calculation of the proposed model (curve a) and measurement either with (curve b) or without (curve c) tissues. So, the accuracy of the proposed model is still quite high when RC is blocked within biological tissues. In future work, the effect of biological tissues on mutual inductance should be taken into consideration.

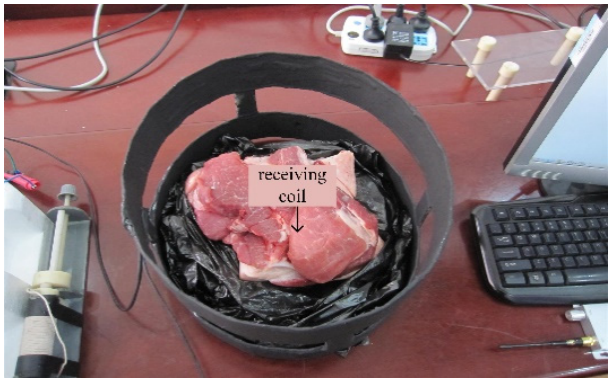

Figure 9. The Setup for measurement of mutual inductance when the receiving coil is tightly surrounded by biological tissues.

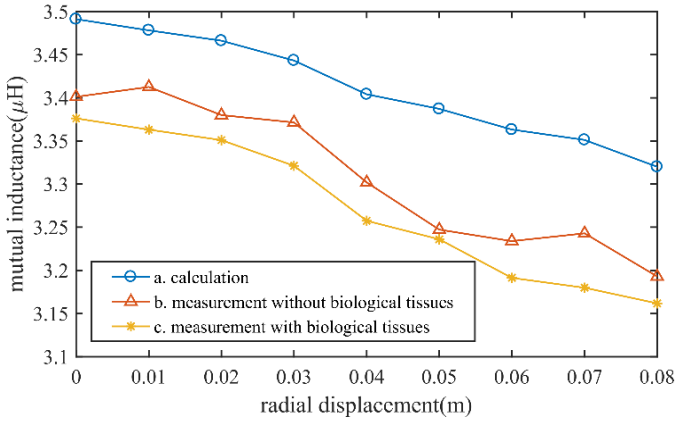

Figure 10. Mutual inductance from calculation of proposed model, measurement with biological tissues, and measurement without tissues.

4. Discussion

4.1. Comparison of the Proposed Mutual Inductance Model with Existing Methods

Common analytic methods can only work out the mutual inductance when directional misalignment is in some particular situations: Such as 45°, 90°, and 135° [25]. The proposed model is applicable for any possible positional and directional misalignment. So only results for positional misalignment can get compared between them. As for directional misalignment, the proposed model is compared with the finite element method (FEM).

FEM is able to obtain mutual inductance in all positional and directional misalignments as long as the mesh of finite elements is tiny enough [26]. However, it is too time-consuming and complicated. The comparison on accuracy and computation time among analytic method, FEM, and proposed mutual inductance model is illustrated in Table 2. In each cell, the first row given is the accuracy, and the second row given is the computation time. The accuracy of the proposed model is higher than the analytic method. Both the accuracy of the proposed model and FEM decreases slightly when directional misalignment happens. The accuracy of FEM is higher than the proposed model to some degree; on the other hand, its computation time is thousands of times larger than the latter. As long as the positional or directional misalignment varies, the FEM should get reworked, which means an infeasible and unacceptable time cost. Considering both the accuracy and computation time, the proposed model reaches a good tradeoff.

Table 2. Accuracy (first row) and computation time (second row) of mutual inductance under various positional and directional misalignments by analytic method, FEM (finite element method), and the proposed model.

$(x, y, z); (\theta,\varphi)$	Ref. [25], Analytic		Ref. [26], FEM		Proposed Model	
	Acc	**Time**	**Acc**	**Time**	**Acc**	**Time**
(0, 0, 0); (0°, 0°)	90.85%	6.79 s	97.39%	1686.97 s	95.93%	2.312 s
(0, 0.03, 0); (0°, 0°)	90.38%	7.35 s	98.28%	1938.94 s	95.21%	2.186 s
(0, 0.06, 0); (0°, 0°)	90.53%	7.51 s	97.94%	1962.33 s	95.62%	2.458 s
(0, 0.10, 0); (0°, 0°)	90.02%	7.85 s	97.15%	2004.81 s	95.81%	2.767 s
(0, 0, 0.03); (0°, 0°)	89.28%	6.98 s	97.04%	1972.89 s	95.03%	2.382 s
(0, 0, 0.06); (0°, 0°)	90.68%	8.35 s	96.28%	2012.45 s	94.78%	2.653 s

Table 2. *Cont.*

(x, y, z); (θ,φ)	Ref. [25], Analytic		Ref. [26], FEM		Proposed Model	
	Acc	Time	Acc	Time	Acc	Time
(0, 0, 0.09); (0°, 0°)	91.26%	10.15 s	97.12%	1983.93 s	94.54%	2.581 s
(0, 0.03, 0.03); (0°, 0°)	90.38%	8.81 s	97.83%	2139.50 s	93.82%	3.419 s
(0, 0.06, 0.06); (0°, 0°)	88.27%	14.57 s	96.26%	2080.58 s	94.16%	3.156 s
(0, 0.10, 0.06); (0°, 0°)	90.06%	16.89 s	96.52%	2339.71 s	93.98%	3.324 s
(0, 0.10, 0.06); (0°,15°)	-		95.56%	3317.68 s	94.28%	5.218 s
(0, 0.10, 0.06); (0°,45°)	-		95.26%	3382.57 s	93.54%	4.972 s
(0, 0.10, 0.06); (0°,75°)	-		96.34%	3658.35 s	93.68%	5.193 s
(0, 0.10, 0.06); (15°, 0°)	-		95.11%	3427.90 s	94.38%	5.622 s
(0, 0.10, 0.06); (45°, 0°)	-		95.42%	3520.03 s	93.73%	5.493 s
(0, 0.10, 0.06); (75°, 0°)	-		97.83%	3486.15 s	94.13%	5.368 s
(0, 0.10, 0.06); (15°,15°)	-		96.17%	3862.42 s	93.56%	6.129 s
(0, 0.10, 0.06); (45°,15°)	-		95.21%	3917.52 s	94.03%	6.217 s
(0, 0.10, 0.06); (45°,45°)	-		95.78%	3885.83 s	93.56%	6.861 s

4.2. Comparison of the Novel Receiving Coil with Existing Coils

For coils with different configuration, their self-inductance varies. So, it is hard to make a distinctive and uniform contrast on mutual inductance between receiving coils in different WPT systems. The coupling coefficient is introduced as following:

$$k_{12} = M_{12} / \sqrt{L_1 L_2} \tag{18}$$

where L_1 and L_2 are the self-inductance of transmitting and receiving coil of the WPT system respectively, and M_{12} is the mutual inductance between them. k_{12} is a normalized parameter and can be utilized to compare coupling performance of different WPT systems.

The performance of coupling and receiving power of the proposed RC with novel structure is compared with existing RCs in different WPT systems, as shown in Table 3. Although the receiving power of the proposed WPT is not the most, both the maximum and minimum of its coupling coefficient are the highest, inferring a most remarkable mutual coupling performance. Additionally, the coupling coefficient of the proposed WPT is stable, which ensures steady and fluent work of WCE. Other WPT systems in [24,27] with higher receiving power but lower coupling efficient indicate a low utilization ratio of energy and excessively high voltage in their TCs, which could do harm to human tissues. The receiving power and coupling coefficient in [28] are too low, even if its RC is the tiniest. The proposed WPT transmit power most efficiently attributes to the special RC.

Table 3. Configuration, receiving power, and coupling coefficient of the proposed and other wireless power transmissions (WPT).

WPT Systems	Size of RC (mm)	Size of WCE (mm)	Frequency (kHz)	Receiving Power (mW)	Min. of k_{12}	Max. of k_{12}
Ref. [24]	Φ 9.5 × 10.0	Φ 12.5 × 26.0	220	508	0.0024	0.0062
Ref. [28]	Φ 9.0 × 6.5	Φ 10.5 × 27.8	16,470	26	0.0006	0.0028
Ref. [27]	12 × 12 × 12	Φ 13.0 × 27.9	250	570	0.0039	0.0110
This study	Φ 12 × 17.3	Φ 12.6 × 24.1	220	394	0.0054	0.0125

It seems that there is no advantage on size of RC for the proposed WPT, compared with other systems. Actually, RC should be capsuled into WCE to obtain sufficient power. So, it is more rational to compare the size of WCE to them instead of size of RC. Thanks to the hollow RC with novel structure allowing other modules of WCE to be put inside it, the proposed WCE has the tiniest size to get through intestines safely and smoothly. In conclusion, the proposed RC uses transmitting coil in the highest utilization ratio, receives sufficient and stable power, and minimizes the size of WCE.

5. Conclusions

For WPT, a hollow cylindrical RC is proposed to supply sufficient power and minimize the size of WCE at the same time. Thanks to its structure and geometry, it receives power from all three dimensions of the electromagnetic field. Neither mutual inductance nor receiving power will vary drastically, no matter how terribly misaligned the RC is. A fast and accurate model on mutual inductance is proposed to study the receiving power in lumped parameter circuits when various positional and directional misalignments happen to RC. The model is validated with a measurement bench. Additionally, measurement of mutual inductance when RC is inside pork tissues indicates that the model is affected slightly by biological tissues. The geometry parameters of RC are specially designed to obtain high mutual inductance for as many misalignments as possible. Standard deviation for mutual inductance of various positional and directional misalignment in the RC is 1.3194 and 1.1747 μH, respectively. It indicates relatively low and smooth variation on receiving power even when the RC is badly misaligned. The performance of the optimal RC is verified with imaging experiment in the GI tract of live pig. Imaging is clear and stable during the whole process. Receiving power is sufficient and stable, even when the position and direction of the RC changes rapidly.

As referred, the effect of biological tissues on mutual inductance should be taken into consideration to improve accuracy for the model in future work. The hollow geometry for coils can also be adopted in other WPT applications with severe constraints in size. The directional factor in Equation (9) can be applied to electromagnetic calculation when directional misalignment exists. The mutual inductance model provides a fast and accurate approach to study coupling related parameters, such as coupling coefficient and receiving power. With sufficient power supply by the novel RC, more advanced functions like drug release are able to be equipped into WCE soon. It makes the reliable clinical application of WCE possible, which would also help reduce epidemics like COVID-19.

Author Contributions: Conceptualization, S.K. and G.Y.; methodology, S.K.; software, Z.W.; validation, S.K., G.Y., and Z.W.; formal analysis, S.K. and Z.W.; investigation, S.K.; resources, G.Y.; data curation, S.K.; writing—original draft preparation, S.K.; writing—review and editing, G.Y.; visualization, Z.W.; supervision, G.Y.; project administration, G.Y.; funding acquisition, G.Y. All authors have read and agreed to the published version of the manuscript.

Ethical Approval: The research related to animal use complied with all the relevant national regulations and institutional policies for the care and use of animals. The study was approved by the Institutional Animal Use and Care Committee of Shanghai Jiao Tong University (SJTU.No20190905AP050631) in 20 September 2019.

Funding: This work was supported by the National Natural Science Foundation of China (NSFC) under Grant 61673271, 81601631, and 81971767, and Foundation of Institute of Medical Robotics, Shanghai Jiao Tong University under Grant IMR2018KY05.

Conflicts of Interest: The authors state no conflict of interest.

Abbreviations

WCE	wireless capsule endoscope
GI	gastrointestinal
WPT	wireless power transmission
TC	transmitting coil
RC	receiving coil
FEM	finite element method

References

1. Wang, J.; Leach, M.; Lim, E.G.; Wang, Z.; Pei, R.; Huang, Y. An Implantable and Conformal Antenna for Wireless Capsule Endoscopy. *IEEE Antennas Wirel. Propag. Lett.* **2018**, *17*, 1153–1157. [CrossRef]
2. Xu, Z.; Shi, L.; Wang, Y.; Zhang, J.; Huang, L.; Zhang, C.; Liu, S.; Zhao, P.; Liu, H.; Zhu, L.; et al. Pathological findings of COVID-19 associated with acute respiratory distress syndrome. *Lancet Respir. Med.* **2020**, *8*, 420–422. [CrossRef]
3. Khan, T.H.; Shrestha, R.; Wahid, K.A.; Babyn, P. Design of a smart-device and FPGA based wireless capsule endoscopic system. *Sens. Actuators A Phys.* **2015**, *221*, 77–87. [CrossRef]
4. Gao, J.; Yan, G. A Novel Power Management Circuit Using a Super-Capacitor Array for Wireless Powered Capsule Robot. *IEEE/ASME Trans. Mechatron.* **2017**, *22*, 1444–1455. [CrossRef]
5. Liu, G.; Yan, G.; Zhu, B.; Lu, L. Design of a video capsule endoscopy system with low-power ASIC for monitoring gastrointestinal tract. *Med. Biol. Eng. Comput.* **2016**, *54*, 1779–1791. [CrossRef]
6. Zhang, H.; Gao, S.-P.; Ngo, T.; Wu, W.; Guo, Y.-X. Wireless Power Transfer Antenna Alignment Using Intermodulation for Two-Tone Powered Implantable Medical Devices. *IEEE Trans. Microw. Theory Tech.* **2019**, *67*, 1708–1716. [CrossRef]
7. Son, D.; Gilbert, H.; Sitti, M. Magnetically Actuated Soft Capsule Endoscope for Fine-Needle Biopsy. *Soft Robot.* **2019**, *7*, 10–21. [CrossRef]
8. Basar, M.R.; Ahmad, M.Y.; Cho, J.; Ibrahim, F. An improved resonant wireless power transfer system with optimum coil configuration for capsule endoscopy. *Sens. Actuators A-Phys.* **2016**, *249*, 207–216. [CrossRef]
9. Bouattour, G.; Elhawy, M.; Naifar, S.; Viehweger, C.; Ben Jmaa Derbel, H.; Kanoun, O. Multiplexed Supply of a MISO Wireless Power Transfer System for Battery-Free Wireless Sensors. *Energies* **2020**, *13*, 1244. [CrossRef]
10. Geng, Y.; Pahlavan, K. Design, Implementation, and Fundamental Limits of Image and RF Based Wireless Capsule Endoscopy Hybrid Localization. *IEEE Trans. Mobile Comput.* **2016**, *15*, 1951–1964. [CrossRef]
11. Han, C.; Zhang, B.; Fang, Z.; Qiu, D.; Chen, Y.; Xiao, W. Dual-Side Independent Switched Capacitor Control for Wireless Power Transfer with Coplanar Coils. *Energies* **2018**, *11*, 1472. [CrossRef]
12. Shang, J.; Yu, Y. An Ultrawideband Capsule Antenna for Biomedical Applications. *IEEE Antennas Wirel. Propag. Lett.* **2019**, *18*, 2548–2551. [CrossRef]
13. He, S.; Yan, G.-Z.; Ke, Q.; Wang, Z.-W.; Chen, W.-W. A wirelessly powered expanding-extending robotic capsule endoscope for human intestine. *Int. J. Precis. Eng. Manuf.* **2015**, *16*, 1075–1084. [CrossRef]
14. Zhou, X.; Chen, B.; Luo, Y.; Zhu, R. Analytical Calculation of Mutual Inductance of Finite-Length Coaxial Helical Filaments and Tape Coils. *Energies* **2019**, *12*, 566. [CrossRef]
15. Hui, Q.; Jin, K.; Zhu, X. Directional Radiation Technique for Maximum Receiving Power in Microwave Power Transmission System. *IEEE Trans. Ind. Electron.* **2019**, *1*, 6376–6386. [CrossRef]
16. Shao, G.; Guo, Y. Hybrid Wireless Positioning and Charging With Switched Field Helmholtz Coils for Wireless Capsule Endoscopy. *IEEE Trans. Microw. Theory Tech.* **2020**, *68*, 904–913. [CrossRef]
17. Khan, S.R.; Desmulliez, M.P. Towards a Miniaturized 3D Receiver WPT System for Capsule Endoscopy. *Micromachines* **2019**, *10*, 545. [CrossRef]
18. Gao, J.; Yan, G. Design and Implementation of a Clamper-Based and Motor-Driven Capsule Robot Powered by Wireless Power Transmission. *IEEE Access* **2019**, *7*, 138151–138161. [CrossRef]
19. Nam, S.J.; Lim, Y.J.; Nam, J.H.; Lee, H.S.; Hwang, Y.; Park, J.; Chun, H.J. 3D reconstruction of small bowel lesions using stereo camera-based capsule endoscopy. *Sci. Rep.* **2020**, *10*, 6025. [CrossRef]
20. Cavlu, V.; Brennan, P. Determining the Position and Orientation of In-Body Medical Instruments Using Near-Field Magnetic Field Mapping. *IEEE J. Electromagn. RF Microw. Med. Biol.* **2020**, *4*, 10–16. [CrossRef]
21. Yin, W.; Lu, M.; Tang, J.; Zhao, Q.; Zhang, Z.; Li, K.; Han, Y.; Peyton, A. Custom edge-element FEM solver and its application to eddy-current simulation of realistic 2M-element human brain phantom. *Bioelectromagnetics* **2018**, *39*, 604–616. [CrossRef] [PubMed]
22. Feng, Y.J.; Chen, X.Y.; Chen, Y.; Li, M.Y.; Zeng, L.; Xie, Q. Numerical Calculation and Experimental Verification of Inductance and Critical Current Characteristics in a Solenoidal SMES Magnet. *IEEE Trans. Appl. Supercond.* **2019**, *29*, 1–5. [CrossRef]
23. Liu, G.; Yan, G.; Xu, W.; Kuang, S. Dual-head wireless powered video capsule based on new type of receiving coils. *J. Med. Eng. Technol.* **2015**, *39*, 246–25224. [CrossRef] [PubMed]

24. Ke, Q.; Luo, W.; Yan, G.; Yang, K. Analytical Model and Optimized Design of Power Transmitting Coil for Inductively Coupled Endoscope Robot. *IEEE Trans. Biomed. Eng.* **2016**, *63*, 694–706. [CrossRef] [PubMed]
25. Tavakkoli, H.; Abbaspour-Sani, E.; Khalilzadegan, A.; Abazari, A.M.; Rezazadeh, G. Mutual inductance calculation between two coaxial planar spiral coils with an arbitrary number of sides. *Microelectron. J.* **2019**, *85*, 98–108. [CrossRef]
26. Rezmerita, G.; Bobaru, L.; Stanculescu, M.; Iordache, M.; Niculae, D. A self and mutual inductance calculation resonators with finite element analysis. In Proceedings of the 2017 International Conference on Modern Power Systems (MPS), Cluj-Napoca, Romania, 6–9 June 2017; pp. 1–4.
27. Basar, M.R.; Ahmad, M.Y.; Cho, J.; Ibrahim, F. An Improved Wearable Resonant Wireless Power Transfer System for Biomedical Capsule Endoscope. *IEEE Trans. Ind. Electron.* **2018**, *65*, 7772–7781. [CrossRef]
28. Na, K.; Jang, H.; Ma, H.; Bien, F. Tracking Optimal Efficiency of Magnetic Resonance Wireless Power Transfer System for Biomedical Capsule Endoscopy. *IEEE Trans. Microw. Theory Tech.* **2015**, *63*, 295–304. [CrossRef]